

# Ground-state and spectral properties of an asymmetric Hubbard ladder

Anas Abdelwahab and Eric Jeckelmann

*Institut für Theoretische Physik, Leibniz Universität Hannover, Appelstr. 2, 30167 Hannover, Germany*

Martin Hohenadler

*Institut für Theoretische Physik und Astrophysik, Universität Würzburg, Am Hubland, 97074 Würzburg, Germany*

(Dated: April 21, 2015)

We investigate a ladder system with two inequivalent legs, namely a Hubbard chain and a one-dimensional electron gas. Analytical approximations, the density matrix renormalization group method, and continuous-time quantum Monte Carlo simulations are used to determine ground-state properties, gaps, and spectral functions of this system at half-filling. Evidence for the existence of four different phases as a function of the Hubbard interaction and the rung hopping is presented. First, a Luttinger liquid exists at very weak interchain hopping. Second, a Kondo-Mott insulator with spin and charge gaps induced by an effective rung exchange coupling is found at moderate interchain hopping or strong Hubbard interaction. Third, a spin-gapped paramagnetic Mott insulator with incommensurate excitations and pairing of doped charges is observed at intermediate values of the rung hopping and the interaction. Fourth, the usual correlated band insulator is recovered for large rung hopping. We show that the wave numbers of the lowest single-particle excitations are different in each insulating phase. In particular, the three gapped phases exhibit markedly different spectral functions. We discuss the relevance of asymmetric two-leg ladder systems as models for atomic wires deposited on a substrate.

PACS numbers: 71.10.Fd, 71.10.Pm, 71.27.+a

## I. INTRODUCTION

Correlated electrons on ladder lattices have been extensively investigated in the last two decades [1–14], but relatively little attention has been paid to asymmetric ladders with two inequivalent legs. The one-dimensional (1D) Kondo-Heisenberg model is the most studied asymmetric ladder system. It was used to investigate exotic superconducting correlations in stripe-ordered high-temperature superconductors [15–18] as well as quantum phase transitions in heavy-fermion materials [19]. Additionally, a two-band Hubbard model on a ladder lattice was the starting point of an investigation of pairing mechanisms in strongly repulsive fermion systems [20].

In a different context, asymmetric ladder systems have been proposed as models for linear atomic wires deposited on the surface of a substrate [21, 22]. In that case, one leg represents the wire while the second leg mimics those degrees of freedom of the substrate that couple to the wire. The study of such models provides a first approximation for the influence of the substrate on hallmarks of 1D physics such as the Peierls instability [21] and the Luttinger liquid [22]. However, this approach has not been pursued systematically until now.

1D electron systems have been studied extensively for more than 60 years [23]. Well-established theories predict various anomalous properties of strictly 1D electron systems such as the Peierls instability [24, 25], incommensurate charge- and spin-density waves [25], the dynamical separation of spin and charge excitations, and the Luttinger liquid behavior of 1D conductors [1]. Experimentally, quasi-1D electron systems have been realized in strongly anisotropic bulk materials such as Bech-

gaard salts [26] and  $\pi$ -conjugated polymers [27]. Experimental and theoretical investigations have both demonstrated that even a weak coupling between 1D electron systems can play an essential role for their physical properties [1, 23, 26].

More recently, quasi-1D electron systems have been realized in atomic wires deposited on the surface of a semiconducting substrate [21, 28, 29]. For instance, it has been claimed that a Peierls metal-insulator transition occurs in indium chains on a silicon substrate [29] and that Luttinger liquid behavior is found in gold chains on a germanium substrate [30]. However, these claims remain controversial. A fundamental issue is that we have a poor theoretical knowledge of the influence of the coupling between wire and substrate. As investigations of interacting electrons on three-dimensional lattices with complex geometries are extremely difficult, the modeling of wire-substrate systems by much simpler asymmetric ladders [21, 22] appears very promising.

In this paper, we consider a two-leg ladder system made of two inequivalent legs; one is an interacting electron system described by the 1D Hubbard model with on-site interaction  $U$  and hopping integral  $t_{\parallel}$ , the other is a 1D electron gas (Fermi gas) described by a tight-binding model with the same  $t_{\parallel}$ . The legs are coupled by an interchain (or rung) hopping  $t_{\perp}$ . This is the simplest model of a correlated atomic wire coupled to a noninteracting substrate. It can also be seen as a special case of the general two-band Hubbard model used to investigate pairing mechanisms [20]. The model is further related to the Kondo-Heisenberg model [15–19] because the Hubbard chain at half-filling has the same low-energy spin excitations as a Heisenberg chain. Thus, the asymmetric

Hubbard ladder can be seen as a generalization of the Kondo-Heisenberg model (which corresponds to a Mott insulator with infinitely large charge gap on the interacting leg) to the case of a Mott insulator with a finite gap for charge excitations.

Here, we investigate the model properties for various values of the interaction  $U$  and the rung hopping  $t_{\perp}$  in a half-filled ladder, as well as at low doping away from half-filling. Ground-state properties, excitation gaps, and spectral functions are determined accurately using the density-matrix renormalization group (DMRG) technique [31–33] and quantum Monte Carlo (QMC) simulations [34]. Furthermore, approximate analytical methods (perturbation theory and mean-field approximation) are used to facilitate the interpretation of the numerical results. We find that the physics of the half-filled asymmetric ladder is very rich, with similarities to the Kondo-Heisenberg model [15–19] and the half-filled symmetric Hubbard ladder [1–5] (corresponding to a ladder with two identical legs) in certain parameter regimes. Furthermore, our results confirm that our model is a good starting point to investigate an atomic wire deposited on a substrate, but also reveal the limitations of representing the substrate by a single chain.

The paper is structured as follows: In Sec. II, we introduce the model and discuss its properties in limiting cases. The Hartree-Fock approximation for half-filling is presented in Sec. III. In Sec. IV, we discuss our DMRG results for the ground-state properties and excitation gaps, while the QMC spectral functions are presented in Sec. V. Finally, Sec. VI contains our conclusions.

## II. MODEL

The Hamiltonian of the asymmetric ladder model takes the form (see also Fig. 1)

$$\begin{aligned}
 H = & -t_{\parallel} \sum_{x,y,\sigma} \left( c_{x+1,y,\sigma}^{\dagger} c_{x,y,\sigma} + c_{x,y,\sigma}^{\dagger} c_{x+1,y,\sigma} \right) \\
 & -t_{\perp} \sum_{x,\sigma} \left( c_{x,F,\sigma}^{\dagger} c_{x,H,\sigma} + c_{x,H,\sigma}^{\dagger} c_{x,F,\sigma} \right) \\
 & + U \sum_x \left( n_{x,H,\uparrow} - \frac{1}{2} \right) \left( n_{x,H,\downarrow} - \frac{1}{2} \right). \quad (1)
 \end{aligned}$$

Here,  $c_{x,y,\sigma}$  ( $c_{x,y,\sigma}^{\dagger}$ ) is an annihilation (creation) operator for an electron with spin  $\sigma$  on the site with coordinates  $(x, y)$  where  $y = H$  (Hubbard leg) or  $y = F$  (Fermi leg) and the rung index  $x$  runs from 1 to the ladder length  $L$ . The corresponding electron number operators are denoted as  $n_{x,y,\sigma} = c_{x,y,\sigma}^{\dagger} c_{x,y,\sigma}$ . Half-filling corresponds to  $N = 2L$  electrons on the ladder. The Hamiltonian is invariant under the particle-hole transformation  $c_{x,y,\sigma} \rightarrow (-1)^x c_{x,y,\sigma}^{\dagger}$ . Therefore, at half-filling its Fermi energy is always equal to 0 and it is sufficient to consider electron fillings  $N \geq 2L$ . We will investigate repulsive interactions ( $U \geq 0$ ) only. As the canonical gauge transformation  $c_{x,H,\sigma} \rightarrow -c_{x,H,\sigma}$ ,  $c_{x,F,\sigma} \rightarrow c_{x,F,\sigma}$  merely changes

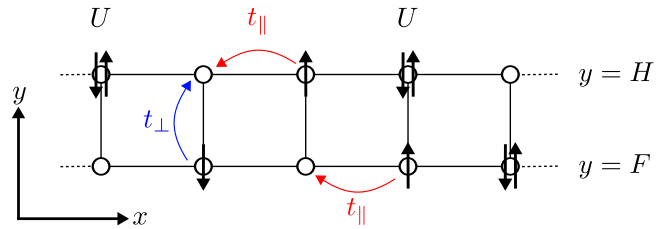


FIG. 1. (Color online) The asymmetric Hubbard ladder described by Hamiltonian (1), with intrachain hopping  $t_{\parallel}$  and interchain hopping  $t_{\perp}$ . On the lower (Fermi,  $y = F$ ) leg, electrons do not interact, whereas on the upper (Hubbard,  $y = H$ ) leg, they experience an onsite repulsion  $U$ .

the sign of  $t_{\perp}$ , and another canonical gauge transformation  $c_{x,y,\sigma} \rightarrow (-1)^x c_{x,y,\sigma}$  simply changes the sign of  $t_{\parallel}$ , we only need to consider  $t_{\parallel} \geq 0$  and  $t_{\perp} \geq 0$ . For our numerical results and figures we use the energy unit  $t_{\parallel} = 1$ .

In general, the Hamiltonian (1) is not exactly solvable. However, we can understand some of its properties by considering limiting cases which are amenable to analytical calculations or related to known models.

### A. Weak interactions

In the noninteracting case ( $U = 0$ ), we recover the well-known tight-binding ladder [1]. The Hamiltonian can be diagonalized using bonding and antibonding rung states. For the single-particle eigenstates we obtain a bonding band with dispersion

$$E_b(k) = -t_{\perp} - 2t_{\parallel} \cos(k) \quad (2)$$

and an antibonding band with dispersion

$$E_{ab}(k) = +t_{\perp} - 2t_{\parallel} \cos(k). \quad (3)$$

For periodic boundary conditions, the wave numbers  $k$  in the first Brillouin zone  $[-\pi, \pi]$  are given by  $k = \frac{2\pi}{L}z$  with an integer  $z$  fulfilling  $-\frac{L}{2} < z \leq \frac{L}{2}$ .

For  $t_{\perp} > 2t_{\parallel}$  the ladder spectrum has an indirect gap

$$E_{\text{band}} = 2t_{\perp} - 4t_{\parallel} \quad (4)$$

between the wave numbers  $k_b = \pm\pi$  in the bonding band and  $k_{ab} = 0$  in the antibonding band, see Fig. 2(a). Consequently, the ladder system is a band insulator at half-filling while it is metallic with two Fermi points at other band fillings. Perturbation theory could be used for weak interactions  $U \ll E_{\text{gap}}$ , but this case is much easier to analyze in the dimer limit (see Sec. IID).

For  $t_{\perp} < 2t_{\parallel}$  the ladder spectrum is gapless and has four perfectly nested Fermi points if the system is at or close to half-filling, see Fig. 2(b). At half-filling the Fermi points  $\pm k_b$  ( $\frac{\pi}{2} < k_b < \pi$ ) and  $\pm k_{ab}$  ( $0 < k_{ab} < \frac{\pi}{2}$ ) are determined by the equation

$$t_{\perp} = -2t_{\parallel} \cos(k_b) = 2t_{\parallel} \cos(k_{ab}) \quad (5)$$

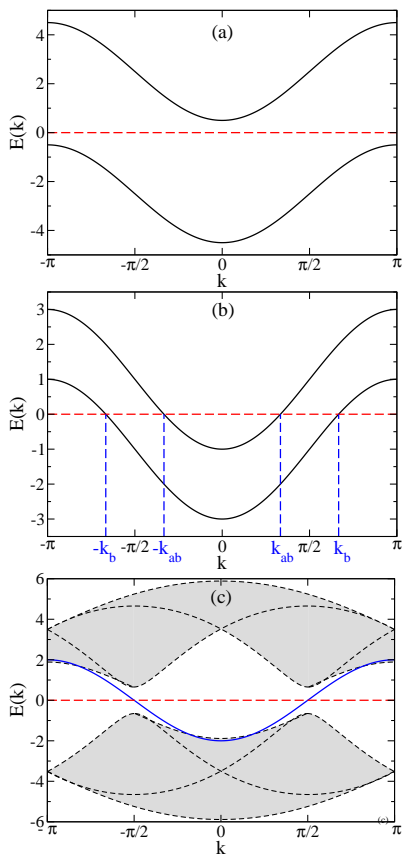


FIG. 2. (Color online) Single-particle dispersions [Eqs. (2) and (3)] of the noninteracting ladder for (a)  $t_{\perp} = 2.5t_{\parallel}$ , (b)  $t_{\perp} = t_{\parallel}$ ; (b) also shows the four Fermi points  $\pm k_{ab}$  and  $\pm k_b$  defined by Eq. (5). (c) Single-particle dispersion of the tight-binding chain (solid blue line) and single holon-spinon continuum (shaded area) of the half-filled Hubbard chain with  $U = 4t_{\parallel}$  from the Bethe ansatz solution. A horizontal dashed line shows the Fermi energy at half-filling in all three figures.

with the nesting wave number  $\pi = k_b + k_{ab}$ . The case of weak interactions  $U \ll t_{\perp}, t_{\parallel}$  could be investigated using sophisticated field-theoretical approaches (bosonization and the renormalization group), as done for symmetric ladders [1, 3, 6–9]. However, for any finite  $U$  the model (1) is no longer symmetric under reflection in the rung direction. The lower symmetry makes field-theoretical calculations much more difficult and, as far as we know, no such calculation has been carried out successfully for asymmetric Hubbard ladders yet. Based on the known results for symmetric ladders [1–3, 5–9], we expect that the excitation spectrum of the half-filled asymmetric ladder becomes fully gapped as soon as  $U > 0$  because the perfect nesting of its Fermi points (with nesting wave number  $\pi$ ) allows for umklapp scattering. The system is then a spin-gapped paramagnetic Mott insulator and its lowest single-particle excitations should occur at four incommensurate wave numbers  $\pm k_g$  and  $\pm k'_g$  with  $k_g \approx k_b$  and  $k'_g \approx k_{ab}$ .

## B. Strong interactions

For  $t_{\perp} = t_{\parallel} = 0$ , electrons are localized and the ground-state is highly degenerate. At or close to half-filling, there is exactly one electron on each site of the Hubbard leg. The other electrons are distributed arbitrarily on the Fermi leg. Using perturbation theory for small but finite hopping terms ( $t_{\perp}, t_{\parallel} \ll U$ ) we find in first order that the intrachain hopping term  $t_{\parallel}$  delocalizes the electrons on the Fermi leg and thus restores a 1D electron gas with a unique ground state. The ground state of the Hubbard leg remains unchanged in first order but second-order corrections yield the usual antiferromagnetic exchange coupling  $J_{\parallel} = 4t_{\parallel}^2/U$  between electrons localized on nearest-neighbor sites (and thus an effective 1D Heisenberg model). The interchain coupling term  $t_{\perp}$  yields a constant energy contribution in second order and thus the legs remain decoupled. Therefore, it seems that the strong-interaction limit is a special case of weakly-coupled chains (see Sec. II C). However, second-order perturbation results are misleading because divergent contributions appear at higher orders in  $t_{\perp}$ .

The problem at hand is very similar to the single-impurity Anderson model. Therefore, we can derive an effective Hamiltonian by using a Schrieffer-Wolff transformation [35]. Without a hopping term  $t_{\parallel}$  in the Hubbard leg, the asymmetric ladder model (1) would be equivalent to a 1D periodic Anderson model and the Schrieffer-Wolff transformation (up to the second order) would lead to a Kondo lattice model [36] with an antiferromagnetic exchange interaction  $J_{\perp} = 8t_{\perp}^2/U$ . With a hopping term  $t_{\parallel} \neq 0$  in both legs, we obtain additional second-order interaction terms: an antiferromagnetic exchange coupling  $J_{\parallel} = 4t_{\parallel}^2/U$  between nearest-neighbor sites in the Hubbard leg, and next-nearest-neighbor correlated hopping terms between Fermi and Hubbard legs of order  $t_{\parallel}t_{\perp}/U$ . Without these correlated hopping terms, the second-order effective Hamiltonian would be the Kondo-Heisenberg model [15–19, 37]. Hence, the asymmetric ladder with strong Hubbard interaction can be seen as a generalization of the Kondo-Heisenberg model to Mott insulators with finite charge gaps. However, correlated hopping terms are known to be important in the strong-coupling limit of Hubbard-type models [38], in particular in two-leg ladders [5]. Therefore, contrary to claims in the literature [17], the strong-interaction limit of the asymmetric ladder (1) is not exactly equivalent to the Kondo-Heisenberg model. However, the Kondo-Heisenberg model could be realized in the strong-coupling limit of a simple generalization of Hamiltonian (1), for instance by introducing a different intrachain hopping  $t_{\parallel}^y$  on each leg.

Nevertheless, for large  $U$  we expect the half-filled asymmetric Hubbard ladder to exhibit similar low-energy physics as the half-filled Kondo-Heisenberg model with exchange couplings  $J_{\perp}, J_{\parallel} \ll t_{\parallel}$ . In the latter model, the rung exchange induces not only a gap for spin excita-

tions but also for charge excitations in the Fermi leg [17] because of umklapp scattering associated with perfect nesting of its Fermi points  $k_F = \pm\frac{\pi}{2}$ . Additionally, the interaction  $U$  is responsible for a large Mott-Hubbard gap on the Hubbard leg of the asymmetric Hubbard ladder model. We will call this state a Kondo-Mott insulator.

### C. Chain limit

For  $t_\perp = 0$ , the model (1) reduces to two independent chains. The first leg corresponds to a 1D electron gas with a nearest-neighbor tight-binding Hamiltonian that can be easily diagonalized. The second leg is a Hubbard chain which is exactly solvable by the Bethe ansatz [39]. If the ladder system is at or close to half-filling, the Hubbard leg is exactly half filled because only electronic states of the Fermi leg are close to the Fermi energy, see Fig. 2(c). Then, the Hubbard leg is a Mott-Hubbard insulator with a charge gap  $E_H$  but gapless spin excitations. The velocity of spin excitations is smaller than  $2t_\parallel$  and decreases with increasing  $U/t_\parallel$ . The other electrons are on the Fermi leg, which is close to be half filled and has two Fermi points  $k_F \approx \pm\frac{\pi}{2}$  with a Fermi velocity  $v_F \approx 2t_\parallel$ . Therefore, the asymmetric ladder system is metallic, with independent low-energy charge and spin excitations. Charge excitations are localized on the Fermi leg while spin excitations have a lower velocity on the Hubbard leg than on the Fermi leg.

The interchain hopping term  $t_\perp$  transfers electrons from one chain to the other and hence creates excitations with energy larger than  $E_H/2$ . Consequently, for  $t_\perp \ll E_H$ , a perturbative treatment is possible but merely yields corrections to the eigenenergies because the ground state is not degenerate. However, we expect the interplay of the Hubbard interaction and the interchain hopping to induce effective interactions for the electrons in the Fermi leg, as observed for the strong-interaction limit (see Sec. II B). The effects of these effective interactions are not known *a priori* but, since a Hubbard chain at half-filling has the same low-energy spin correlations as a Heisenberg chain, we expect the low-energy physics of the weakly coupled chains to be similar to the Kondo-Heisenberg model with an effective rung exchange coupling  $J_\perp \propto t_\perp^2/E_H \ll E_H, t_\parallel$ .

For weak to moderate interactions  $U \lesssim 4t_\parallel$ , the charge gap  $E_H$  remains small and charge fluctuations between the legs are not negligible. Thus one cannot assume that the Fermi leg is exactly half filled. For the Kondo-Heisenberg model away from half-filling, various ground states such as Luttinger liquids (with gapless charge and spin excitations) and spin-gapped phases with gapless charge excitations have been found [15, 17, 19, 37]. Nonetheless, we should recover an effective model with a half-filled Fermi leg for sufficiently large  $U$ , as discussed in Sec. II B. Therefore, various scenarios are possible for the half-filled asymmetric Hubbard ladder in the limit of weakly-coupled chains. On the one hand, we expect that

the ladder system remains gapless and thus becomes a Luttinger liquid for some range of the parameters  $(U, t_\perp)$ . On the other hand, for large enough  $U$ , we should recover a Kondo-Mott insulator with nonzero spin and charge gaps. Other states are also possible, as suggested by the studies of the Kondo-Heisenberg model away from half-filling [15, 17, 19, 37]. In all cases, the lowest single-particle excitations should remain at the wave numbers given by the Fermi points of the 1D electron gas, in particular,  $k_g = \pm\frac{\pi}{2}$  for any gapped phase. In principle, field theory [7, 8, 16, 17] could be used to investigate the effects of weak interchain coupling more rigorously.

### D. Dimer limit

For  $t_\parallel = 0$ , we can decompose the Hamiltonian (1) into a sum of independent two-site Hamiltonians that act on one rung each and can be easily diagonalized. If the ladder system is half filled, the ground state corresponds to each rung being occupied by two electrons that form a spin singlet. The lowest spin excitation with energy

$$E_s^{\text{dimer}} = -\frac{U}{4} + \sqrt{\left(\frac{U}{4}\right)^2 + 4t_\perp^2} \quad (6)$$

corresponds to the formation of a triplet on one rung. The lowest charge excitation with energy

$$E_c^{\text{dimer}} = -2\sqrt{\left(\frac{U}{4}\right)^2 + t_\perp^2} + 2\sqrt{\left(\frac{U}{4}\right)^2 + 4t_\perp^2} \quad (7)$$

corresponds to moving an electron from one rung to the other. We note that  $E_s^{\text{dimer}} \approx E_c^{\text{dimer}} \approx 2t_\perp$  for  $U \ll t_\perp$  in agreement with the weak-interaction analysis for the band insulating case ( $t_\perp > 2t_\parallel$ ) in Sec. II A, while  $E_c^{\text{dimer}} \approx \frac{12t_\perp^2}{U} > E_s^{\text{dimer}} \approx \frac{8t_\perp^2}{U}$  for  $U \gg t_\perp$  in agreement with the rung exchange coupling deduced for strong interactions in Sec. II B. If we dope the ladder system away from half-filling by adding electrons, some of the rungs become occupied by three electrons in the ground state and both spin and charge gaps drop immediately to zero.

For small but finite  $t_\parallel$  we can use perturbation theory as long as  $t_\parallel \ll E_s^{\text{dimer}}, E_c^{\text{dimer}}$  which corresponds to an energy scale  $\sim t_\perp$  for weak interactions ( $U \ll t_\perp$ ) and to  $\sim t_\perp^2/U$  for strong interactions ( $U \gg t_\perp$ ). This gives an effective hopping  $t_\parallel^{\text{eff}} \propto t_\parallel$  and an effective attractive interaction  $V_\parallel^{\text{eff}} \propto t_\parallel^2/E_c^{\text{dimer}}$  between nearest-neighbor rungs. In summary, the half-filled asymmetric ladder in the dimer limit is a correlated band insulator for large enough  $t_\perp/U$ . For large  $U/t_\perp$ , it may be regarded as a Kondo-Mott insulator with spin and charge gaps induced by an effective rung exchange coupling, as discussed in Secs. II B and II C.

### III. HARTREE-FOCK APPROXIMATION

To gain a better (qualitative) understanding of the asymmetric ladder model at half-filling, we apply the Hartree-Fock approach for Hubbard-type interactions [40] to Hamiltonian (1) and obtain the spin-dependent single-particle Hamiltonians

$$\begin{aligned}
H_\sigma = & -t_\parallel \sum_{x,y} \left( c_{x,y,\sigma}^\dagger c_{x+1,y,\sigma} + c_{x+1,y,\sigma}^\dagger c_{x,y,\sigma} \right) \\
& -t_\perp \sum_x \left( c_{x,H,\sigma}^\dagger c_{x,F,\sigma} + c_{x,F,\sigma}^\dagger c_{x,H,\sigma} \right) \\
& + U \sum_x n_{x,H,\sigma} \left( \langle n_{x,H,-\sigma} \rangle - \frac{1}{2} \right), \quad (8)
\end{aligned}$$

where the expectation value of the density on the Hubbard leg  $\langle n_{x,H,-\sigma} \rangle$  must be calculated self-consistently for the ground state of  $H_{-\sigma}$ . The Hartree-Fock approximation is a method for weak interactions  $U$ .

As discussed in Sec. II A, the Fermi points are perfectly nested by an interband wave number  $k = \pi$  at half-filling and for  $t_\perp < 2t_\parallel$ . Therefore, the most probable symmetry breaking is an antiferromagnetic spin-density wave

$$\langle n_{x,H,\sigma} \rangle = \frac{1}{2} + \sigma(-1)^x \frac{m_H}{2} \quad (9)$$

with the staggered magnetization (per site) of the Hubbard leg,  $m_H$ , as the order parameter. Consequently, the unit cell of the effective Hamiltonian (8) is twice as large as that of the original Hamiltonian (1) in the leg direction and contains four sites. According to Bloch's theorem, the single-particle Hamiltonians (8) can be diagonalized by a canonical transformation of the form

$$\begin{aligned}
d_{k,n,\sigma}^\dagger = & \frac{1}{\sqrt{L}} \sum_x e^{ikx} \left\{ [u_{kn\sigma} + (-1)^x v_{kn\sigma}] c_{x,H,\sigma}^\dagger \right. \\
& \left. + [s_{kn\sigma} + (-1)^x t_{kn\sigma}] c_{x,F,\sigma}^\dagger \right\} \quad (10)
\end{aligned}$$

with the normalization condition

$$|u_{kn\sigma}|^2 + |v_{kn\sigma}|^2 + |s_{kn\sigma}|^2 + |t_{kn\sigma}|^2 = 1 \quad (11)$$

and a wave number  $k$  in a reduced Brillouin zone  $[-\frac{\pi}{2}, \frac{\pi}{2}]$ , i.e.,  $k = \frac{2\pi}{L}z$  with  $-\frac{L}{4} < z \leq \frac{L}{4}$ . The index  $n = 1, 2, 3, 4$  numbers the four bands. The four components  $\mathbf{V}_{kn\sigma} = (u_{kn\sigma}, v_{kn\sigma}, s_{kn\sigma}, t_{kn\sigma})$  are the solutions of the four-dimensional eigenvalue problem

$$H_{k\sigma} \mathbf{V}_{kn\sigma} = \epsilon_{n\sigma}(k) \mathbf{V}_{kn\sigma} \quad (12)$$

with the Hamiltonian matrix  $H_{k\sigma}$  given by

$$\begin{pmatrix}
-2t_\parallel \cos(k) & -\frac{1}{2}\sigma U m_H & -t_\perp & 0 \\
-\frac{1}{2}\sigma U m_H & +2t_\parallel \cos(k) & 0 & -t_\perp \\
-t_\perp & 0 & -2t_\parallel \cos(k) & 0 \\
0 & -t_\perp & 0 & +2t_\parallel \cos(k)
\end{pmatrix}$$

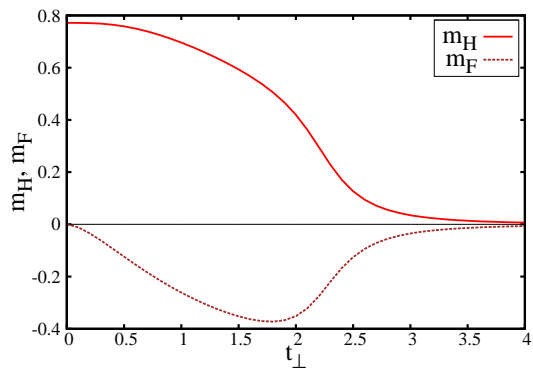


FIG. 3. (Color online) Staggered magnetization of the Hubbard leg ( $m_H$ ) and Fermi leg ( $m_F$ ) for  $U = 4t_\parallel$  in the Hartree-Fock approximation as a function of the rung hopping  $t_\perp$ .

and the single-particle (Hartree-Fock) eigenenergy  $\epsilon_{n\sigma}(k)$ . The staggered magnetization is given by

$$m_H = \sigma \frac{4}{L} \sum_{n=1}^2 \sum_k u_{kn\sigma} v_{kn\sigma}, \quad (13)$$

where the first sum runs over the lowest two bands only. Equations (12) and (13) constitute a self-consistency problem which can be easily solved numerically.

As expected for a 1D system with a perfect nesting of the Fermi points, we find a broken-symmetry solution  $m_H \neq 0$  for any  $U > 0$  if  $t_\perp < 2t_\parallel$ . Furthermore, this staggered magnetization seems to remain stable even for larger  $t_\perp$  (at least up to  $4t_\parallel$ ) although  $m_H$  becomes quite small. However, the long-range antiferromagnetic order is an artifact of the mean-field approximation since the continuous  $SU(2)$  spin symmetry can not be spontaneously broken in one dimension [1, 40]. In Fig. 3 we show the self-consistent order parameter  $m_H$  obtained for  $U = 4t_\parallel$  as a function of the rung hopping  $t_\perp$ . (Qualitatively similar results are found for other values of  $U$ .) As expected,  $m_H$  approaches the value obtained for the 1D Hubbard model [40] for  $t_\perp \rightarrow 0$  and its absolute value decreases monotonically with increasing  $t_\perp$ . Although there is no direct electron-electron interaction on the Fermi leg, the coupling to the Hubbard leg induces an antiferromagnetic spin-density wave. The corresponding staggered magnetization,

$$m_F = (-1)^x \langle n_{x,F,\uparrow} - n_{x,F,\downarrow} \rangle, \quad (14)$$

is also shown in Fig. 3. We see that  $m_F$  is not a monotonic function of the interchain coupling  $t_\perp$ . It vanishes for  $t_\perp = 0$  because the Fermi leg is just an independent electron gas in that case (see Sec. II C). The initial increase of  $|m_F|$  with  $t_\perp$  reflects the enhanced hybridization of electronic states on the two legs while the final decrease mirrors the diminution of the antiferromagnetic correlations in the Hubbard leg. Note that  $m_H$  and  $m_F$  have opposite signs because of the antiferromagnetic correlations between electrons on the same rung.

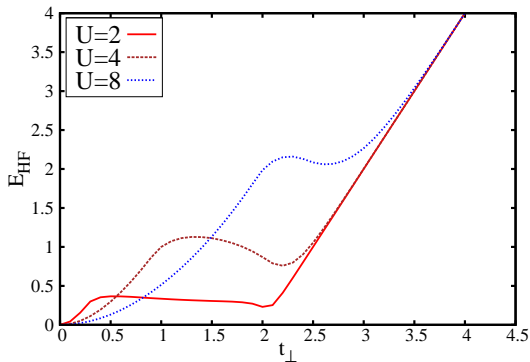


FIG. 4. (Color online) Hartree-Fock gap  $E_{\text{HF}}$  for  $U/t_{\parallel} = 2, 4$  and  $8$  as a function of the rung hopping  $t_{\perp}$ .

The dispersion of the Hartree-Fock eigenenergies can be calculated analytically for a given  $m_{\text{H}}$ . It has the form

$$\epsilon_{n\sigma}(k) = \pm \sqrt{a(k)} \pm \sqrt{b(k)} \text{ with}$$

$$a(k) = \frac{1}{2} \left( \frac{Um_{\text{H}}}{2} \right)^2 + [2t_{\parallel} \cos(k)]^2 + t_{\perp}^2,$$

$$b(k) = \frac{1}{4} \left( \frac{Um_{\text{H}}}{2} \right)^4 + 4t_{\perp}^2 [2t_{\parallel} \cos(k)]^2 + \left( \frac{Um_{\text{H}}}{2} \right)^2 t_{\perp}^2.$$

The four possible combinations of signs correspond to the four bands  $\epsilon_{n\sigma}(k)$ ,  $n = 1, 2, 3, 4$ . (Note that the bands are identical for  $\sigma = \pm 1$ .)

The Hartree-Fock gap  $E_{\text{HF}}$  is defined as the lowest excitation energy when the Hartree-Fock bands are half filled, i.e., as the energy difference between the lowest state in the third-lowest band and the highest state in the second-lowest band. As expected, this gap vanishes if  $U = 0$  or  $t_{\perp} = 0$ . If both couplings are finite, however, we find that the Hartree-Fock gap is always larger than zero. The gap has a surprisingly complex dependence on the interaction strength and the rung hopping, as illustrated in Fig. 4. We observe three different regions as a function of  $t_{\perp}$ . First, the gap is small but increases rapidly with  $t_{\perp}$ , then it reaches a local maximum at intermediate values of  $t_{\perp}$  and decreases slowly until it reaches a local minimum at some value  $t_{\perp} > 2t_{\parallel}$ . Finally, it increases linearly with  $t_{\perp}$  at large values of  $t_{\perp}$ . The behavior at large  $t_{\perp}$  is easy to understand from the discussion of the noninteracting (Sec. II A) and dimer limits (Sec. II D). Indeed, we see that for large  $t_{\perp}$  the Hartree-Fock gap approaches the band gap given by Eq. (4). In this region, the Hartree-Fock solution can be regarded as a band insulator with a weak, incidental antiferromagnetic ordering. In the other two regions, however, the antiferromagnetic ordering is responsible for the gap opening. These Hartree-Fock solutions describe antiferromagnetic Mott insulators [40]. For a weak rung hopping the Hartree-Fock gap increases systematically with  $U$ . This case is related to the spin-density-wave insulator with modulation  $2k_F = \pi$  which is found in the Hartree-Fock approximation for 1D half-filled Hubbard-type models. Note that the extent of the

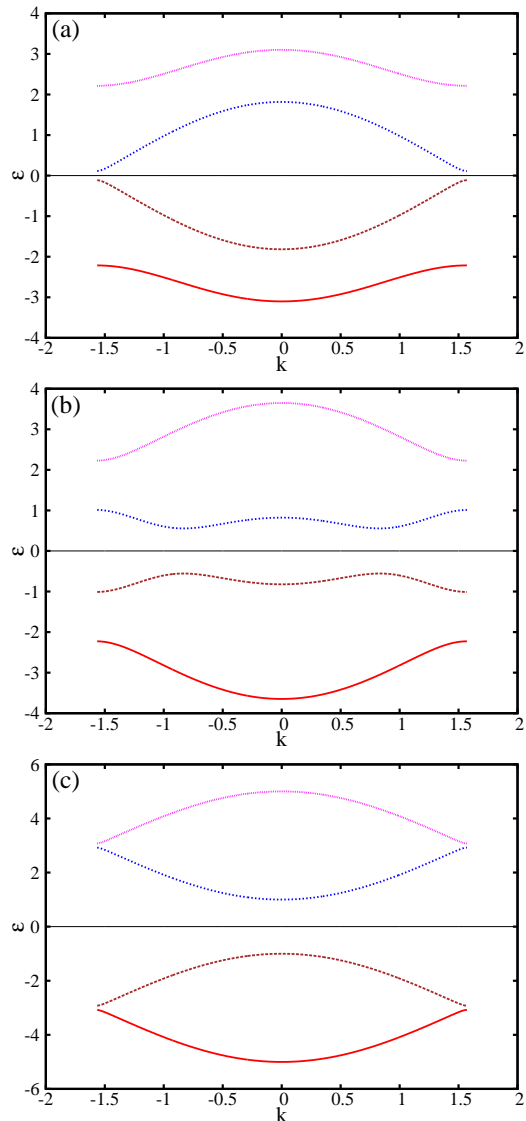


FIG. 5. (Color online) The four Hartree-Fock bands  $\epsilon_{n\sigma}(k)$  for  $U = 5t_{\parallel}$  with (a) weak ( $t_{\perp} = 0.5t_{\parallel}$ ), (b) intermediate ( $t_{\perp} = 1.5t_{\parallel}$ ), and (c) strong ( $t_{\perp} = 3t_{\parallel}$ ) rung hopping.

intermediate region in terms of  $t_{\perp}$  decreases upon increasing the interaction  $U$ .

The qualitative difference between the first two regions (weak to moderate rung hopping) is revealed by studying the features of the Hartree-Fock dispersions  $\epsilon_{n\sigma}(k)$ . They are shown in Fig. 5 for a self-consistent staggered magnetization  $m_{\text{H}}$  at  $U = 5t_{\parallel}$ . For a weak rung hopping [see Fig. 5(a)] the lowest single-particle excitations are located at the edge of the reduced Brillouin zone ( $k_{\text{HF}} = \pm \frac{\pi}{2}$ ), in agreement with the analysis of weakly-coupled chains in Sec. II C. Figure 5(b) shows that the lowest excitations correspond to single-particle states with incommensurate wave numbers  $k_{\text{HF}}$  in the intermediate regime in agreement with the analysis of the case  $t_{\perp} < 2t_{\parallel}$  and weak interaction  $U$  in Sec. II A. The wave number  $k_{\text{HF}}$  determined from the Hartree-Fock so-

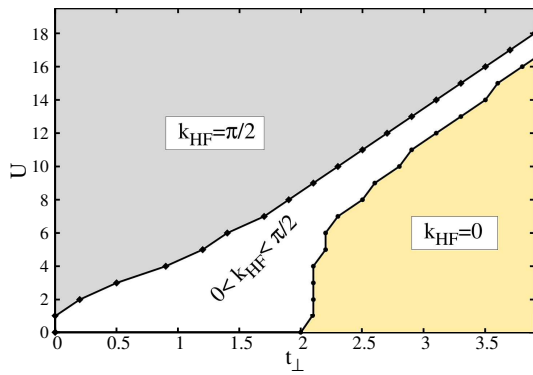


FIG. 6. (Color online) Hartree-Fock “phase diagram” in the  $(U, t_{\perp})$  plane with three different regions. The lowest single-particle excitations have wave numbers  $k_{\text{HF}}$  at the edges of the reduced Brillouin zone ( $k_{\text{HF}} = \pm\frac{\pi}{2}$ ), at its center ( $k_{\text{HF}} = 0$ ), and at incommensurate values  $0 < |k_{\text{HF}}| < \frac{\pi}{2}$ , respectively.

lution shifts progressively from the edges of the reduced Brillouin zone ( $k_{\text{HF}} = \pm\frac{\pi}{2}$ ) to its center ( $k_{\text{HF}} = 0$ ) with increasing  $t_{\perp}$ , in qualitative agreement with the incommensurate wave number given by Eq. (5). Finally, for a strong rung hopping  $t_{\perp}$  [see Fig. 5(c)], the lowest excitations are localized in the center of the reduced Brillouin zone. This result also agrees with the analysis of the case  $t_{\perp} > 2t_{\parallel}$  and weak interaction  $U$  in Sec. II A. The indirect gap between  $k_g = \pm\pi$  and  $k'_g = 0$  found there [see Fig. 2(a)] becomes a direct gap at  $k_{\text{HF}} = 0$  in the Hartree-Fock approximation because of the folding of the Brillouin zone. Finally, the HF “phase diagram” in Fig. 6 shows that all three cases are found over a finite range of the parameters  $(U, t_{\perp})$ .

#### IV. GROUND-STATE PROPERTIES AND EXCITATION GAPS

##### A. DMRG method

To obtain reliable results for the asymmetric ladder Hamiltonian (1) at finite  $U$  and  $t_{\perp}$ , we use the DMRG method [31–33], which has previously been applied to symmetric [2, 5, 10, 32] and asymmetric two-leg ladders [15, 17, 19, 20]. Here, the ground-state properties of Hamiltonian (1) are calculated using the finite-system DMRG algorithm on lattices with up to  $L = 200$  rungs (400 sites) and open boundary conditions. Up to  $m = 3072$  density-matrix eigenstates were kept, yielding discarded weights smaller than  $10^{-6}$ . Truncation errors were investigated systematically by keeping variable numbers of density-matrix eigenstates and ground-state energies were extrapolated to the limit of vanishing discarded weights. The resulting error estimates for gaps are shown in the figures when they are larger than the symbol sizes. We were able to reach a sufficient accuracy for the lowest eigenenergies for all parameters but for

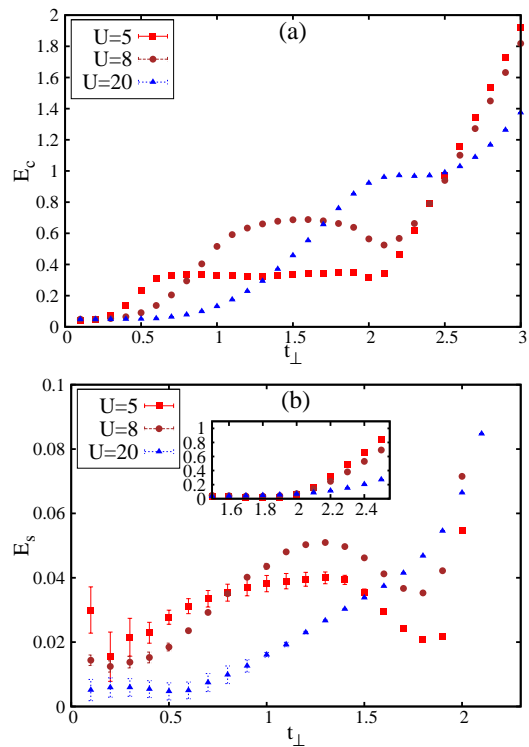


FIG. 7. (Color online) (a) Charge gap  $E_c$  and (b) spin gap  $E_s$  calculated with the DMRG as a function of the rung hopping  $t_{\perp}$  in a half-filled asymmetric two-leg Hubbard ladder with  $L = 128$  rungs. Finite-size corrections are of the order of the symbol size in (a) and of the order of  $0.01t_{\parallel}$  in (b). Error bars indicate DMRG truncation errors larger than the symbol size.

weakly-interacting, weakly-coupled chains with  $U \leq 4t_{\parallel}$  and  $t_{\perp} < 2t_{\parallel}$ . As usual with variational approaches, the accuracy is lower for other observables (density profiles, correlation functions). In some cases, irregular density profiles and correlation functions demonstrate that the DMRG calculation has not fully converged because of (quasi-) degenerate low-lying eigenstates. The relevant cases are discussed below together with our results.

##### B. Excitation energies

In this section, we discuss the excitation gaps calculated for a half-filled asymmetric ladder. The gap for charge excitations in a ladder with  $N = 2M$  electrons is

$$E_c = \frac{1}{2} [E_0(M+1, M+1) + E_0(M-1, M-1) - 2E_0(M, M)], \quad (15)$$

where  $E_0(M_{\uparrow}, M_{\downarrow})$  denotes the ground-state energy of Hamiltonian (1) with  $M_{\sigma}$  electrons of spin  $\sigma$ . It is the gap seen in the dynamical charge structure factor, which can be probed by electron-energy-loss spectroscopy.

Figure 7(a) shows the behavior of the charge gap as a function of the interaction  $U$  and the rung hopping  $t_{\perp}$ ,

which is qualitatively similar to the Hartree-Fock gap  $E_{\text{HF}}$  in Fig. 4. A closer investigation reveals four distinct regions: region (I) for very small  $t_{\perp}$ , where the gap stays at a finite value because of finite-size effects, region (II) where  $E_c$  increases quadratically with  $t_{\perp}$ , region (III) at intermediate  $t_{\perp}$  where the gap saturates (or even decreases), and region (IV) where  $E_g$  increases rapidly with  $t_{\perp}$  and eventually approaches the value of the band gap (4) as expected (see Secs. II A and II D). Region (II) extends to larger values of  $t_{\perp}$  for a stronger interaction  $U$ , while the onset of region (IV) shifts from  $t_{\perp} = 2t_{\parallel}$  to larger values as  $U$  increases.

The gap in region (II) can be well fitted to a function  $f(t_{\perp}) = a + b \frac{4t_{\perp}^2}{U}$ , yielding a slope  $b$  that increases from  $b \approx 1.1$  for  $U = 5t_{\parallel}$  to  $b \approx 1.5$  for  $U = 20t_{\parallel}$ . The scaling of the charge gap with  $t_{\perp}^2$  shows that the gap opening is related to the effective rung exchange coupling  $J_{\perp}$  discussed in Secs. II B and II C. The intercept  $a$  is negative, suggesting that the charge gap could close at a small but finite  $t_{\perp}$ . The condition  $f(t_{\perp}^c) = 0$  yields the critical coupling  $t_{\perp}^c(U)$  below which the charge gap seems to disappear. For instance, we get  $t_{\perp}^c(U = 20t_{\parallel}) \approx 0.85t_{\parallel}$ ,  $t_{\perp}^c(U = 8t_{\parallel}) \approx 0.35t_{\parallel}$ , and  $t_{\perp}^c(U = 5t_{\parallel}) \approx 0.1t_{\parallel}$ . Region (I) corresponds roughly to the domain  $t_{\perp} < t_{\perp}^c(U)$ .

To check the finite-size effects we have performed calculations for ladder lengths from  $L = 20$  to  $L = 200$  and extrapolated the charge gap to  $L \rightarrow \infty$  using a quadratic fit in  $1/L$ .  $E_c$  remains finite in the thermodynamic limit for all parameters  $U, t_{\perp} > 0$ , except for region (I), where the charge gap vanishes as  $E_c \approx 6t_{\parallel}/L$ . For comparison, the exact scaling for a half-filled tight-binding chain is  $E_c = 2\pi t_{\parallel}/L$ . The scaling confirms that added charges (electrons or holes) go primarily on the Fermi leg and that the interchain hopping  $t_{\perp}$  barely affects low-energy charge excitations in the limit of weak  $t_{\perp}$ , see Sec. II C.

The spin gap of a ladder with  $N = 2M$  electrons is

$$E_s = E_0(M + 1, M - 1) - E_0(M, M), \quad (16)$$

and corresponds to the excitation gap in the dynamical spin structure factor. It can be measured using inelastic neutron scattering. Its behavior as a function of  $U$  and  $t_{\perp}$  is shown in Fig. 7(b). We see that it is qualitatively similar to that of the charge gap, although the difference between regions (II) and (III) is less clear. In addition, for large enough  $t_{\perp}$ , both gaps approach the value of the band gap (4), as expected. For smaller  $t_{\perp}$ , the spin gap is generally (much) smaller than the charge gap.

Finite-size scaling reveals that the spin gap is finite in the thermodynamic limit for all parameters  $U, t_{\perp} > 0$ , except for region (I), where  $E_s$  vanishes as  $E_s \approx ct_{\parallel}/L$ . The values of the prefactor  $c = c_{\text{DMRG}}$  as deduced from our DMRG data agree well with the exact values  $c = c_{\text{BA}}$  obtained from the Bethe ansatz (BA) solution for the 1D Hubbard model on an open chain [39]. For instance, for moderate interactions ( $U = 5t_{\parallel}, t_{\perp} = 0.1t_{\parallel}$ ) we get  $c_{\text{DMRG}} \approx c_{\text{BA}} \approx 2.23$ , while for ( $U = 8t_{\parallel}, t_{\perp} = 0.3t_{\parallel}$ ) we obtain  $c_{\text{DMRG}} \approx 1.49$  vs.  $c_{\text{BA}} \approx 1.51$ , and for strong interactions ( $U = 20t_{\parallel}, t_{\perp} = 0.5t_{\parallel}$ ) we find  $c_{\text{DMRG}} \approx 0.681$

vs.  $c_{\text{BA}} \approx 0.637$ . This scaling confirms that the lowest triplet excitation is essentially a spin excitation of the Hubbard leg and that the interchain hopping  $t_{\perp}$  barely affects it in the limit of weak  $t_{\perp}$ , see Sec. II C. Moreover, the different prefactors for the finite-size charge and spin gaps are a signature of the dynamical separation of charge and spin excitations (i.e., different charge and spin velocities) in the infinite ladder system.

The single-particle gap for a ladder with  $N = 2M$  electrons is defined as

$$E_p = E_0(M + 1, M) + E_0(M - 1, M) - 2E_0(M, M). \quad (17)$$

This is the gap for the excitations seen in the single-particle spectral function discussed in Sec. V and experimentally accessible by angle-resolved photoemission spectroscopy. We find that  $E_p$  equals the charge gap for weak and strong rung hopping but differs significantly from it in the intermediate regime. The difference

$$E_{\text{pb}} = 2(E_p - E_c) \quad (18)$$

is called the pair binding energy and is shown in Fig. 8(a). A significant binding energy only exists for moderate interactions  $5t_{\parallel} \lesssim U \lesssim 8t_{\parallel}$  and intermediate rung hoppings  $0.5t_{\parallel} \lesssim t_{\perp} \lesssim 2.0t_{\parallel}$ . This corresponds roughly to region (III) where both charge and spin gaps saturate or decrease with increasing  $t_{\perp}$ . The study of finite-size effects confirms that  $E_{\text{pb}}$  remains finite in the limit of infinite ladder length. In the other three regions, the pair binding energy is very small or negative and vanishes in the thermodynamic limit.

It is interesting to study the effect of charges added to the half-filled system. Upon doping, the charge and spin gaps close within the accuracy of our calculations (limited by finite-size effects and truncation errors). However, the single-particle gap seems to remain finite at low doping in region (III) as shown in Fig. 8(b) for  $t_{\perp} = t_{\parallel}$ . In the other regions, the pair binding energy is negligible or even negative, as illustrated in the same figure for the case  $t_{\perp} = 3t_{\parallel}$  that corresponds to region (IV). Pairing of added charges also occurs in half-filled symmetric Hubbard ladders, but with a finite spin gap [2, 5].

Our results for the excitation energies, together with the analysis of limiting cases in Sec. II, seem to suggest the existence of (at least) four distinct phases in the parameter space ( $U > 0, t_{\perp} > 0$ ) of the half-filled asymmetric Hubbard ladder. In region (I), i.e., for very small rung hopping  $t_{\perp}$ , we find gapless charge and spin excitations. This corresponds to the Luttinger liquid phase which is expected in the limit of weakly coupled chains, see Sec. II C. In region (II), i.e., for moderate  $t_{\perp}$  or strong repulsion  $U$ , the charge gap increases quadratically with  $t_{\perp}$  or, equivalently, linearly with an effective rung exchange coupling  $J_{\perp}$ . The spin gap also increases with  $t_{\perp}$  but its scaling with  $J_{\perp}$  is less clear and it is smaller than the charge gap. We identify this phase with the Kondo-Mott insulator defined in Secs. II B and II C. In region (III), i.e., for intermediate values of  $t_{\perp}$  and  $U$ , both charge and

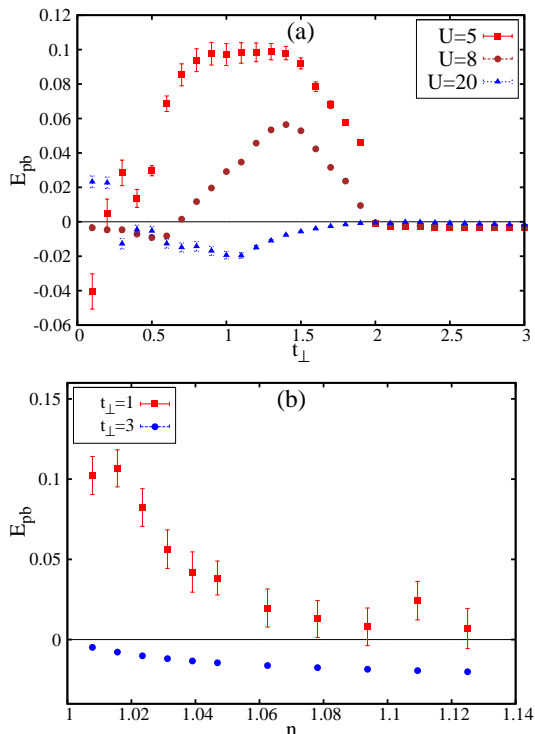


FIG. 8. (Color online) Pair binding energy  $E_{pb}$  calculated with DMRG in an asymmetric two-leg Hubbard ladder with  $L = 128$  rungs (a) as a function of the rung hopping  $t_{\perp}$  at half-filling for several values of the Hubbard interaction  $U$  and (b) as a function of the band filling  $n = N/2L$  for  $U = 5t_{\parallel}$  and two values of  $t_{\perp}$ . Finite-size corrections are smaller than  $0.05t_{\parallel}$ . Error bars indicate DMRG truncation errors larger than the symbol size.

spin gaps are finite but exhibit nonmonotonic behavior with increasing rung hopping. This phase is characterized by a charge gap much larger than the spin gap, and by a pair binding energy of the same order of magnitude as the spin gap. This is consistent with a spin-gapped paramagnetic Mott insulator (similar to the state found in half-filled symmetric Hubbard two-leg ladders [1–5]) which is expected to exist in the weak-interaction limit of the asymmetric ladder (see Sec. II A). Finally, in region (IV), i.e., for large  $t_{\perp}$ , both charge and spin gaps increase monotonically with the rung hopping and approach the band gap (4) for large enough  $t_{\perp}$ . Region (IV) corresponds to a correlated band insulator. Indeed, the onset of this phase is at  $t_{\perp} = 2t_{\parallel}$  in the weak-interaction limit (as seen in Sec. II A) and increases to larger rung hoppings  $t_{\perp}$  for stronger interactions  $U$ , as observed in the discussion of the dimer limit in Sec. II D.

Strictly speaking, our DMRG results for the excitation gaps only demonstrate the existence of two phases (a gapless one and a gapped one) in the half-filled asymmetric Hubbard ladder. The distinction between three different insulating phases has been motivated mainly by the analysis of limiting cases in Sec. II and the similarity with the results of the Hartree-Fock approximation in

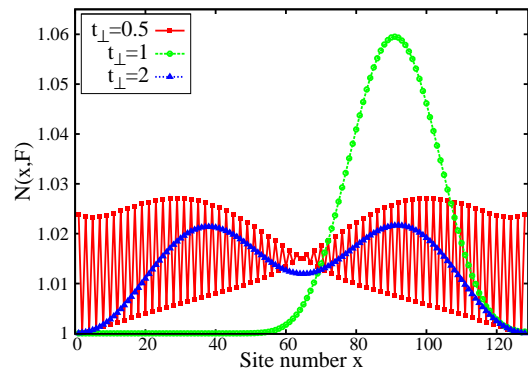


FIG. 9. (Color online) Ground-state charge density distribution on the Fermi leg for two electrons added to a half-filled ladder with  $U = 8t_{\parallel}$  and three values of  $t_{\perp}$ .

Sec. III. In addition, it should be kept in mind that we have not obtained reliable DMRG data when both the interaction and the rung hopping are small, i.e.,  $U \leq 4t_{\parallel}$  and  $t_{\perp} < 2t_{\parallel}$ . Hence, the distinction between the three insulating phases remains rather tentative so far. We now turn to the density profiles of excitations, and later to the single-particle spectral functions, to demonstrate that the phase diagram indeed includes three qualitatively different gapped phases.

### C. Density profiles

At half-filling, the asymmetric ladder exhibits uniform charge and spin densities. Other ground-state expectation values such as bond correlations also show some structure as a result of the open boundary conditions used, but we have not found any significant pattern while varying the model parameters  $t_{\perp}$  and  $U$ . However, we have obtained much information from the charge- and spin-density variations associated with the excitations discussed in the previous sections (added electrons/holes and triplet spin excitations). First of all, the density variations confirm that added charges go primarily on the Fermi leg while a triplet spin excitation is mostly localized on the Hubbard leg. This bias becomes larger with stronger interaction  $U$  but decreases when the rung hopping increases, which is consistent with our analysis of the various limiting cases in Sec. II.

The variations of the charge density along the legs also provide us with useful information about the different phases. For instance, Fig. 9 shows the ground-state charge density on the Fermi leg,

$$N(x, F) = \langle \psi | n_{x,F} | \psi \rangle, \quad (19)$$

where  $n_{x,y} = n_{x,y,\uparrow} + n_{x,y,\downarrow}$  and  $|\psi\rangle$  denotes the ground state, when two electrons are added to a half-filled ladder with  $U = 8t_{\parallel}$ . We clearly see three qualitatively different density profiles. In the Kondo-Mott insulator phase ( $t_{\perp} = 0.5t_{\parallel}$ ), the density distribution of the added

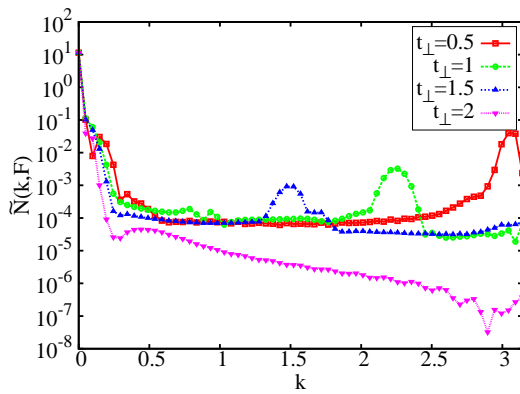


FIG. 10. (Color online) Fourier transform of the ground-state charge density on the Fermi leg with two electrons added to a half-filled ladder with  $U = 5t_{\parallel}$  and four values of  $t_{\perp}$ .

charges oscillates strongly from one site to the next. (Similar patterns exist in the Luttinger liquid phase but the results are less clear-cut because of larger DMRG errors.)

In the spin-gapped Mott insulator phase ( $t_{\perp} = t_{\parallel}$ ), both added charges are concentrated in a single wave packet on one side of the system as if they were bound together. This confirms the tendency to binding added charges revealed by the pair binding energy in the previous section. This charge distribution breaks the reflection symmetry around the center of the Fermi leg, which indicates that odd and even excitations are degenerate, at least within the accuracy of our DMRG calculation. We also observe spin and charge densities that break the reflection symmetry if a single electron is added to the half-filled ladder. In that case, the symmetry breaking is readily explained by the degeneracy of the lowest single-particle excitations with wave numbers  $k_g$  and  $k'_g$ , see Sec. V. In an open chain with an even number of sites, the condition  $k_g + k'_g = \pi$  (see Sec. II A) implies that one of this state is even while the other one is odd with respect to a reflection. Thus the DMRG algorithm may return any (symmetry-breaking) linear combination of these two states for the ground state. We think that a similar (quasi-) degeneracy occurs for two-particle excitations. (We have also investigated the ground state with up to 32 electrons added to a half-filled  $2 \times 128$  ladder and found no sign of phase separation.)

In the correlated band insulator phase ( $t_{\perp} = 2t_{\parallel}$ ), the added charges appear to be independent. Actually, their density distribution corresponds to two free particles in a tight-binding box. In conclusion, the distinct density profiles for added charges confirm the existence of three different gapped phases and the tendency for pair binding in the spin-gapped Mott insulating phase.

A more quantitative study can be made using the Fourier transform of these density distributions. For instance, Fig. 10 shows the Fourier transform of the charge

density on the Fermi leg,

$$\tilde{N}(k, F) = \frac{1}{\sqrt{L}} \left| \sum_{x=1}^L N(x, F) \exp(-ikx) \right| \quad (20)$$

for  $k = 2\pi z/L$  with integers  $|z| < L/2$ , when two electrons are added to a half-filled ladder with  $U = 5t_{\parallel}$ . The strong peak around  $k = 0$  is mostly due to the uniform density of the half-filled system. If the lowest elementary single-charge excitations have wave numbers  $\pm k_g$  then  $\tilde{N}(k, F)$  should exhibit peaks at  $k = \pm 2k_g \pmod{2\pi}$ . We see in Fig. 10 that the residual spectral weight is concentrated close to  $k = \pi$  for the Kondo-Mott insulator ( $t_{\perp} = 0.5t_{\parallel}$ ). This implies that the lowest excitations have a wave number  $k_g = \pi/2$  in this phase. In the spin-gapped Mott insulator (cf. data for  $t_{\perp} = t_{\parallel}$  and  $1.5t_{\parallel}$  in Fig. 10) the spectral weight exhibits peaks at wave numbers  $0 < |q| < \pi$ . This suggests that the low-energy excitations have incommensurate wave numbers  $k_g = |q|/2$  and  $k'_g = \pi - |q|/2$  in that phase. Finally, in the correlated band insulator phase ( $t_{\perp} = 2t_{\parallel}$  in Fig. 10) we observe no other structure than the  $k = 0$  peak. This corresponds to low-energy excitations with wave numbers  $k_g = 0$  or  $\pi$ .

Similarly, we have studied the spin distribution of the lowest triplet eigenstate as well as the charge and spin distributions for one added electron. All results are compatible with the above analysis: low-energy single-particle excitations have wave numbers  $\pm\pi/2$  in the Luttinger liquid and Kondo-Mott insulator, incommensurate wave numbers in the spin-gapped Mott insulator, and wave numbers 0 or  $\pi$  in the correlated band insulator. These results also agree perfectly with the analysis of the limiting cases in Sec. II.

Somewhat surprisingly, the presence of three gapped phases with distinct low-energy excitations is correctly predicted by the Hartree-Fock approximation, see Sec. III. However, the latter is otherwise quite inaccurate as it predicts an antiferromagnetic Mott insulator or a band insulator with antiferromagnetic long-range order for all parameters  $U, t_{\perp} > 0$ , while the (almost exact) DMRG results confirm the absence of any antiferromagnetic long-range order (and also reveal the existence of an additional, gapless phase).

#### D. Correlation functions

The DMRG method has been used to compute static correlation functions of ladder systems [2, 8, 32, 33]. Unfortunately, their interpretation can be rather difficult because of the open boundary conditions. In the asymmetric Hubbard ladder (1), it is further complicated by the different behavior of the two legs. Nevertheless, we calculated, e.g., charge-charge and spin-spin correlations as well as various singlet and triplet pairing correlations. Typically, we can obtain accurate results for small system lengths  $L$ , or for short distances  $x$ , but long-distance

correlations are quite inaccurate because of an insufficient DMRG convergence. Thus we have not succeeded in gaining much useful information for the asymptotic behavior of correlation functions.

In the Luttinger liquid phase, we find dominant anti-ferromagnetic spin correlations with a power-law decay  $x^\alpha$  and exponents  $\alpha$  close to  $-1$ , as in a half-filled Hubbard chain. In the correlated band insulator phase, with its large charge and spin gaps, we observe that all correlations decay exponentially. In the two other phases (Kondo-Mott and spin-gapped Mott insulators), however, we find a rapid (faster than  $x^{-2}$ ) but apparently nonexponential decay of correlation functions. Clearly, in those cases, the correlation lengths are larger than our system sizes (up to  $L = 128$  rungs) and we do not see the asymptotic behavior.

We also investigated correlation functions of the asymmetric Hubbard ladder away from half-filling to understand the nature of the charge pairing observed when electrons or holes are added to a half-filled ladder in the spin-gapped Mott insulating phase. Unfortunately, we do not find any enhanced pairing correlations and hence do not understand the structure of these pairs. Among all the pairing correlation functions that we examined, pair-density-wave (PDW) correlations [17] decrease most slowly. PDW correlations in two-leg ladder systems have attracted much interest recently [8, 17, 18, 41, 42] because they resemble correlations in the PDW state which was proposed to describe the phenomenology of stripe-ordered high-temperature superconductors. Interestingly, dominant quasi-long range PDW correlations have been found in a spin-gapped phase of the Kondo-Heisenberg model away from half-filling [17]. In the asymmetric Hubbard ladder close to half-filling, however, we find that PDW correlation functions decay as  $x^{-2}$  or faster with distance  $x$ . The dominant correlations seem to be power-law charge and spin correlations with exponents  $\alpha$  between  $-1$  and  $-2$ . For comparison, in the symmetric Hubbard ladder close to half-filling, the dominant pairing correlations are of the  $d$ -wave type but they are not enhanced, i.e., they decay as  $x^{-2}$  like for a non-interacting ladder ( $U = 0$ ) [2, 5].

## V. SPECTRAL FUNCTIONS

Our analysis of excitation density profiles in Sec. IV C and the Hartree-Fock approximation in Sec. III suggests that the lowest elementary excitations have different wave numbers  $k_g$  in the three gapped phases that exist at half-filling. To confirm this hypothesis, we consider the momentum and energy-resolved single-particle spectral function, which can be probed experimentally using angle-resolved photoemission spectroscopy. The sharp maxima at the spectrum onset in correlated electron systems [7, 43, 44] allows us to determine  $k_g$ .

Although the single-particle spectral function can in principle be calculated with the DMRG method [43, 44],

such calculations come at a high computational cost and the interpretation of the results is complicated by the use of pseudo-wave numbers for open boundary conditions. (For instance, we can see in Fig. 10 that peaks of a Fourier spectrum are still considerably smeared by boundary effects even for large ladders with 128 rungs.) Instead, we calculate the spectral function using the CT-INT continuous-time quantum Monte Carlo method [34], which is based on a weak-coupling expansion in the interaction  $U$ , and gives exact results for finite systems and finite temperatures. A detailed review of the method has been given in Ref. [45]. We used single-vertex updates and Ising spin flips, and simulated ladders with periodic boundary conditions along the legs.

With the help of the stochastic maximum entropy method [46], we can perform the necessary analytic continuation of the QMC results for the single-particle Green function  $G(k, y, \tau) = \langle c_{k,y,\sigma}^\dagger(\tau) c_{k,y,\sigma}(0) \rangle$  to obtain the single-particle spectral function

$$A(k, y, \omega) = \frac{1}{Z} \sum_{ij} |\langle i | c_{k,y,\sigma} | j \rangle|^2 (e^{-\beta E_i} + e^{-\beta E_j}) \times \delta(\Delta_{ji} - \omega). \quad (21)$$

Here,  $c_{k,y,\sigma}$  is the Fourier transform of  $c_{x,y,\sigma}$  in the leg direction,  $Z$  is the grand-canonical partition function,  $|i\rangle$  is an eigenstate with energy  $E_i$ , and  $\Delta_{ji} = E_j - E_i$ . We carried out simulations for closed-shell configurations ( $L = 30$ ) and open-shell configurations ( $L = 32$ ) at inverse temperatures  $\beta t_{\parallel} = 30$  and  $32$ , respectively. We did not observe any significant finite-size effect for the wave number of the lowest excitations. The analytical continuation introduces some quantitative uncertainties, but the overall features of the spectral functions are robust and fully agree with the results obtained above. Because closed-shell results are usually more reliable and more representative of the thermodynamic limit, we only report the latter below.

QMC methods were used to study spectral functions of symmetric ladders in Refs. [4, 11, 12]. Because symmetric ladders conserve the parity under reflection in the rung direction, the spectral function was investigated separately for the bonding and antibonding orbitals. For the asymmetric ladder studied here, it is more convenient to consider the spectral function for the Hubbard and Fermi legs separately, as indicated by  $y$  in Eq. (21). As a result of the particle-hole symmetry of Hamiltonian (1) at half-filling,  $A(k, y, \omega)$  has the symmetry property  $A(k, y, -\omega) = A(k + \pi, y, \omega)$ . Consequently, the single-particle gap is symmetric around  $\omega = 0$ . In addition, the system is symmetric under a reflection in the leg direction and thus  $A(-k, y, \omega) = A(k, y, \omega)$ .

The spectral functions for the Hubbard and Fermi legs in the four different phases of the model (1) are shown in Fig. 11. The interaction is fixed to  $U = 5t_{\parallel}$ , while the hopping  $t_{\perp}$  increases from top to bottom, leading to a progression from weakly coupled chains to a true ladder system with strong rung hopping.

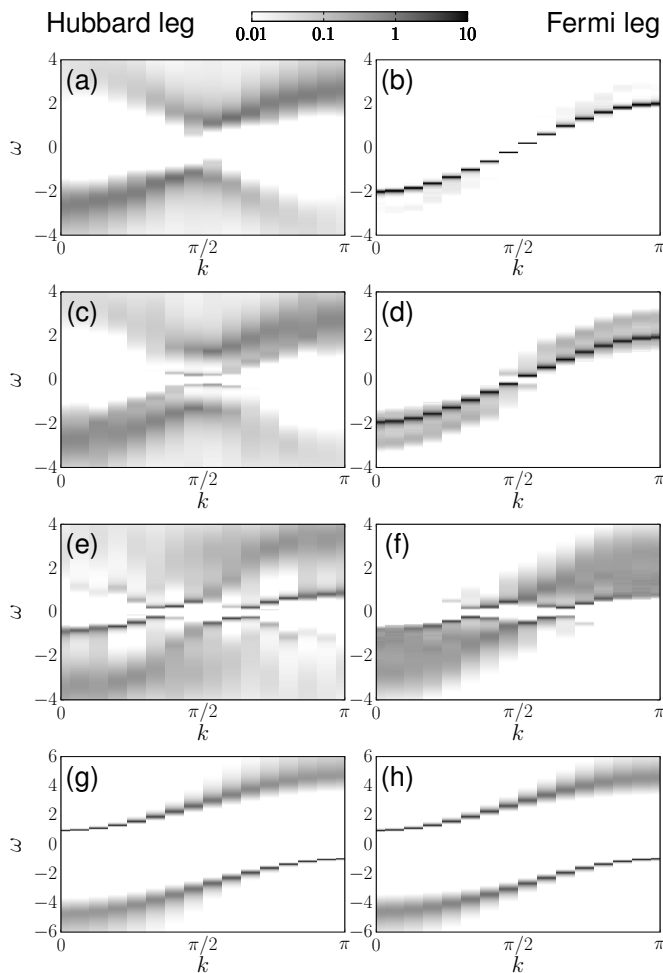


FIG. 11. Spectral functions  $A(k, y, \omega)$  on the Hubbard leg (left column) and the Fermi leg (right column) calculated using the CT-INT method with  $\beta t_{\parallel} = 30$  on a periodic ladder with  $L = 30$  rungs and  $U = 5t_{\perp}$ . (a),(b) Luttinger liquid phase ( $t_{\perp} = 0.1t_{\parallel}$ ), (c),(d) Kondo-Mott insulator ( $t_{\perp} = 0.3t_{\parallel}$ ), (e),(f) incommensurate spin-gapped Mott insulator ( $t_{\perp} = t_{\parallel}$ ), (g),(h) correlated band insulator ( $t_{\perp} = 3t_{\parallel}$ ).

In the Luttinger liquid phase, Figs. 11(a) and (b), the spectrum on the Hubbard leg looks clearly different from the free-particle like spectrum on the Fermi leg. There is substantial weight at  $\omega = 0$  for the Fermi wave number  $k_F = \pi/2$ , indicating metallic behavior. Away from  $\omega = 0$  the main spectral features still reflect the dispersion of elementary excitations in independent chains, compare with Fig. 2(c).

For the Kondo-Mott insulator phase [see Figs. 11(c) and (d)] the lowest excitations are clearly located at  $k_g = \pi/2$ . The gap is not visible because the true gap expected from the DMRG calculations is only a pseudogap as a result of the finite temperature used in the CT-INT simulations. Nevertheless, all results in Fig. 11 are compatible with our findings for the DMRG single-particle gap (17). The spectral function of the Hubbard leg in

Fig. 11(c) resembles that of a Hubbard chain [43, 44] while the spectral function of the Fermi leg [Fig. 11(d)] looks quite similar to Fig. 11(b) but with signs of the pseudogap at  $\omega = 0$ ,  $k = \pi/2$ .

For the spin-gapped Mott phase we see in Figs. 11(e) and (f) that the lowest excitations are at wave numbers  $k_g$  and  $k'_g$ , which are quite symmetrically located around  $\pi/2$ , so that  $k_g + k'_g \approx \pi$ . Thus, in this intermediate regime of  $t_{\perp}$ , the lowest single-particle excitations have incommensurate wave numbers. Incommensurability in the excitation spectrum has also been found in the half-filled symmetric Hubbard ladder with moderate rung hopping [2], in a frustrated Kondo-Heisenberg model [19], and in various correlated 1D systems such as the bilinear biquadratic spin-1 chain [47] and a two-leg spin ladder with nearest and next-nearest coupling [13, 14]. In contrast to the DMRG, the CT-INT method also yields accurate results for weak on-site repulsion  $U$ , and shows that an incommensurate excitation spectrum exists down to at least  $U = 3t_{\parallel}$  for  $t_{\perp} = t_{\parallel}$ . We suspect that this phase remains as  $U \rightarrow 0$  and could be investigated with field-theoretical approaches starting from a noninteracting asymmetric ladder, as discussed in Sec II A.

Finally, in the correlated band insulator regime shown in Figs. 11(g) and (h), the lowest excitations have wave number  $k_g = \pi$  for particle removal and  $k_g = 0$  for particle addition, respectively. The spectra are almost identical on the two legs. This agrees with the analysis of the weak-interaction limit in Sec. II A [compare with Fig. 2(a)] and the dimer limit in Sec. II D. Indeed, when  $t_{\perp}$  is large enough, elementary excitations become almost (anti-)symmetric with respect to a reflection in the rung direction. Obviously, this case is very similar to a half-filled symmetric Hubbard ladder with a strong rung hopping.

The markedly distinct spectral functions in Fig. 11 confirm the existence of one metallic and three different gapped phases in the asymmetric Hubbard ladder at half-filling. The phases can be characterized by the wave numbers of the low-energy excitations, in agreement with the analysis of limiting cases, the Hartree-Fock approximation, and the DMRG density profiles.

## VI. CONCLUSIONS

In this work, we studied the rich physics of the half-filled asymmetric ladder model (1). In particular, we found three gapped phases that differ in the shape of their single-particle excitation spectra, in addition to a Luttinger liquid phase. For strong Hubbard interaction  $U$  or weak interchain hopping  $t_{\perp}$ , our model is related to the Kondo-Heisenberg model, whereas for weak Hubbard repulsion  $U$  or strong rung hopping  $t_{\perp}$ , it is similar to that of a half-filled symmetric Hubbard ladder. Although we do not have enough data to draw a quantitative phase diagram, we show in Fig. 12 a schematic and tentative phase diagram that summarizes our findings. Surpris-

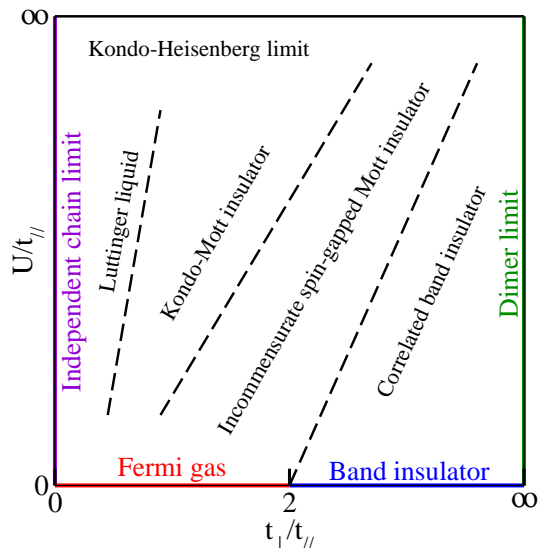


FIG. 12. (Color online) Schematic phase diagram of the half-filled asymmetric Hubbard ladder.

ingly, the overall structure is similar to the Hartree-Fock “phase diagram” in Fig. 6 including, in particular, the wave numbers of the lowest single-particle excitations. The main differences are the presence of a Luttinger liquid phase at small interchain hopping and the absence of long-range antiferromagnetic order.

The three gapped phases are not differentiated by a symmetry breaking or a gap closing but only by a change of the wave number of the low-energy excitations. Similar transitions between phases with commensurate and incommensurate low-energy excitations were found previously in other models, such as the bilinear-biquadratic spin-1 chain [47]. It is difficult to determine phase boundaries numerically for phase transitions that do not involve any symmetry breaking or gap closing. In recent years, various measures of entanglement have been proposed as useful tools for the study of quantum phase transitions [48–52]. We examined one of them, the block entropy in the middle of the lattice, using the DMRG method. Although we observed a different scaling of this entropy with block size in the gapless phase compared to the gapped ones, we did not find any feature which could help locate the boundaries between the three gapped phases. Nevertheless, it is likely that DMRG calculations combined with one of the more sophisticated entanglement-based methods could provide a more precise phase diagram.

The existence of a Luttinger liquid phase has been demonstrated within the accuracy of our numerical methods. It should be kept in mind, however, that exponentially small energy scales usually associated with Kondo physics are not accessible with these methods. Therefore, we cannot rigorously exclude the existence of other phases with exponentially small gaps in the limit of very small interchain hopping. We think that the best ap-

proach to solve this issue, and more generally to improve our understanding of the asymmetric Hubbard ladder, is a more systematic investigation of the limiting cases in Sec. II. On the one hand, effective models for the low-energy physics can be derived in the strong-interaction ( $U \gg t_{\parallel}$ ) and dimer ( $t_{\perp} \gg t_{\parallel}$ ) limits. They should be more amenable to our numerical methods and simple analytical approximations and could thus provide us with a better understanding of the upper and right-hand-side parts of the phase diagram in Fig. 12. On the other hand, it is likely that field-theoretical methods for weakly-coupled chains (see Sec. II C) and weakly-interacting ladders (Sec. II A) could be used to investigate the left-hand and lower parts of the phase diagram.

This study was motivated by the problem of correlated quantum wires deposited on a substrate. In this context, our results confirm that 1D correlated systems are extremely sensitive to their environment. Their properties can be drastically modified by varying the strength of the hybridization (the hopping  $t_{\perp}$ ) between the interacting wire (the Hubbard leg) and the noninteracting substrate (the Fermi leg). In that perspective, the study of asymmetric ladder models constitutes a useful approach for exploring the basic physics of a quantum wire deposited on a substrate.

Yet we also face some problems with this approach. Clearly, it is not enough to represent the substrate by a single chain because the wire interaction can then dominate the full system as our results show. Instead, the substrate should include many more explicit degrees of freedom than the wire. This could be realized using wider ladders with several legs representing the substrate. Indeed, it is possible to map the Hamiltonian of some wire-substrate systems exactly onto ladder models with an infinite number of inequivalent legs. (A similar idea has been recently used to map multiple multi-orbital impurities on a honeycomb lattice onto effective multi-leg ladder systems [53].) An effective ladder model with  $n + 1$  legs can then be seen as the “ $n$ -th order” approximation of the substrate degrees of freedom. We think that this approach could enable a more systematic study of wire-substrate systems in the future.

In addition, in most experiments, the substrate is a band insulator. This condition can be easily realized using two or more orbitals per site but this will double the number of model parameters (at least). This reveals the most serious practical difficulty: we do not know which parameter regime is appropriate for real systems such as atomic wires deposited on substrates. Therefore, ladder models cannot currently be used to study specific materials but can only provide generic information about the physics of quasi-1D electron systems. However, we think that systematic studies of effective  $n$ -leg ladder models could enable the determination of appropriate model parameters by comparison with experiments and first-principles simulations for wire-substrate systems.

## ACKNOWLEDGMENTS

We thank R. M. Noack and A. Rosch for helpful discussions. This work has been done as part of the Research Units *Metallic nanowires on the atomic scale: Electronic and vibrational coupling in real world systems* (FOR1700) and *Advanced Computational Methods for Strongly Cor-*

*related Quantum Systems* (FOR1807) of the German Research Foundation (DFG) and was supported by grants Nos. JE 261/1-1 and Ho 4489/2-1. The DMRG calculations were carried out on the cluster system at the Leibniz University of Hannover and at the Sudan Center for HPC and Grid Computing. The QMC simulations were performed at the Jülich Supercomputing Centre.

- 
- <sup>1</sup> T. Giamarchi, *Quantum Physics in One Dimension* (Oxford University Press, Oxford, 2007).
- <sup>2</sup> R. M. Noack, S. R. White, and D. J. Scalapino, Phys. Rev. Lett. **73**, 882 (1994).
- <sup>3</sup> L. Balents and M. P. A. Fisher, Phys. Rev. B **53**, 12133 (1996).
- <sup>4</sup> D. J. Scalapino, Physica C **282-287**, 157 (1997).
- <sup>5</sup> E. Jeckelmann, D. J. Scalapino, and S. R. White, Phys. Rev. B **58**, 9492 (1998).
- <sup>6</sup> D. Controzzi and A. M. Tsvelik, Phys. Rev. B **72**, 035110 (2005).
- <sup>7</sup> A. M. Tsvelik, Phys. Rev. B **83**, 104405 (2011).
- <sup>8</sup> N. J. Robinson, F. H. L. Essler, E. Jeckelmann, and A. M. Tsvelik, Phys. Rev. B **85**, 195103 (2012).
- <sup>9</sup> S. T. Carr, B. N. Narozhny, and A. A. Nersesyan, Annals of Physics **339**, 22 (2013).
- <sup>10</sup> S. R. White, R. M. Noack, and D. J. Scalapino, Phys. Rev. Lett. **73**, 886 (1994).
- <sup>11</sup> T. Dahm and D. J. Scalapino, Physica C **288**, 33 (1997).
- <sup>12</sup> D. J. Scalapino, Physica B **318**, 92 (2002).
- <sup>13</sup> A. Lavarélo, G. Roux, and N. Laflorencie, Phys. Rev. B **84**, 144407 (2011).
- <sup>14</sup> I. T. Shyiko, I. P. McCulloch, J. V. Gumenjuk-Sichevska, and A. K. Kolezhuk, Phys. Rev. B **88**, 014403 (2013).
- <sup>15</sup> A. E. Sikkema, I. Affleck, and S. R. White, Phys. Rev. Lett. **79**, 929 (1997).
- <sup>16</sup> O. Zachar and A. M. Tsvelik, Phys. Rev. B **64**, 033103 (2001).
- <sup>17</sup> E. Berg, E. Fradkin, and S. A. Kivelson, Phys. Rev. Lett. **105**, 146403 (2010).
- <sup>18</sup> A. Dobry, A. Jaefari, and E. Fradkin, Phys. Rev. B **87**, 245102 (2013).
- <sup>19</sup> E. Eidelstein, S. Moukouri, and A. Schiller, Phys. Rev. B **84**, 014413 (2011).
- <sup>20</sup> K. A. Al-Hassanieh, C. D. Batista, P. Sengupta, and A. E. Feiguin, Phys. Rev. B **80**, 115116 (2009).
- <sup>21</sup> M. Springborg and Y. Dong, *Metallic Chains / Chains of Metals* (Elsevier, Amsterdam, 2007).
- <sup>22</sup> I. K. Dash and A. J. Fisher, J. Phys.: Condens. Matter **13**, 5035 (2001).
- <sup>23</sup> D. Baeriswyl and L. Degiorgi (Eds.), *Strong Interactions in Low Dimensions* (Kluwer Academic Publishers, Dordrecht, 2004).
- <sup>24</sup> S. Kagoshima, H. Nagasawa, and T. Sambongi, *One-Dimensional Conductors* (Springer, Berlin, 1982).
- <sup>25</sup> G. Grüner, *Density Waves in Solids* (Perseus Publishing, Cambridge, 2000).
- <sup>26</sup> M. Dressel, ISRN Condens. Matter Phys. **2012**, 732973 (2012).
- <sup>27</sup> H. Kiess (ed.), *Conjugated Conducting Polymers* (Springer, Berlin, 1992).
- <sup>28</sup> N. Oncel, J. Phys.: Condens. Matter **20**, 393001 (2008).
- <sup>29</sup> P. C. Snijders and H. H. Weitering, Rev. Mod. Phys. **82**, 307 (2010).
- <sup>30</sup> C. Blumenstein, J. Schäfer, S. Mietke, S. Meyer, A. Dollinger, M. Lochner, X. Y. Cui, L. Patthey, R. Matzdorf, and R. Claessen, Nature Physics **7**, 776 (2011).
- <sup>31</sup> S. R. White, Phys. Rev. Lett. **69**, 2863 (1992); Phys. Rev. B **48**, 10345 (1993).
- <sup>32</sup> U. Schollwöck, Rev. Mod. Phys. **77**, 259 (2005).
- <sup>33</sup> E. Jeckelmann, in *Computational Many Particle Physics* (Lecture Notes in Physics **739**), edited by H. Fehske, R. Schneider, and A. Weiße (Springer-Verlag, Berlin, Heidelberg, 2008), p. 597.
- <sup>34</sup> A. N. Rubtsov, V. V. Savkin, and A. I. Lichtenstein, Phys. Rev. B **72**, 035122 (2005).
- <sup>35</sup> J. R. Schrieffer and P. A. Wolff, Phys. Rev. **149**, 491 (1966).
- <sup>36</sup> C. Lacroix and M. Cyrot, Phys. Rev. B **20**, 1969 (1979).
- <sup>37</sup> O. Zachar, Phys. Rev. B **63**, 205104 (2001).
- <sup>38</sup> H. Eskes, A. M. Oleś, M. B. J. Meinders, and W. Stephan, Phys. Rev. B **50**, 17980 (1994).
- <sup>39</sup> F.H.L. Essler, H. Frahm, F. Göhmann, A. Klümper, and V. Korepin, *The One-Dimensional Hubbard Model* (Cambridge University Press, Cambridge, 2005).
- <sup>40</sup> F. Gebhard, *The Mott Metal-Insulator Transition* (Springer, Berlin, 1997).
- <sup>41</sup> J. Almeida, G. Roux, and D. Poilblanc, Phys. Rev. B **82**, 041102 (2010).
- <sup>42</sup> A. Jaefari and E. Fradkin, Phys. Rev. B **85**, 035104 (2012).
- <sup>43</sup> H. Benthien, F. Gebhard, and E. Jeckelmann, Phys. Rev. Lett. **92**, 256401 (2004).
- <sup>44</sup> E. Jeckelmann, Progress of Theoretical Physics Supplement **176**, 143 (2008).
- <sup>45</sup> E. Gull, A. J. Millis, A. I. Lichtenstein, A. N. Rubtsov, M. Troyer, and P. Werner, Rev. Mod. Phys. **83**, 349 (2011).
- <sup>46</sup> K. S. D. Beach, arXiv:cond-mat/0403055 (2004).
- <sup>47</sup> O. Golinelli, Th. Jolicœur, and E. S. Sørensen, Eur. Phys. J. B **11**, 199 (1999).
- <sup>48</sup> A. Osterloh, L. Amico, G. Falci, and R. Fazio, Nature **416**, 608 (2002).
- <sup>49</sup> L.-A. Wu, M. S. Sarandy, and D. A. Lidar, Phys. Rev. Lett. **93**, 250404 (2004).
- <sup>50</sup> Ö. Legeza and J. Sólyom, Phys. Rev. Lett. **96**, 116401 (2006).
- <sup>51</sup> Ö. Legeza, J. Sólyom, L. Tincani, and R. M. Noack, Phys. Rev. Lett. **99**, 087203 (2007).
- <sup>52</sup> C. Mund, Ö. Legeza, and R. M. Noack, Phys. Rev. B **79**, 245130 (2009).
- <sup>53</sup> T. Shirakawa and S. Yunoki, Phys. Rev. B **90**, 195109 (2014).